A. Airoldi, S. Fournier, E. Borlandelli, P. Bettini, G. Sala
Design and Manufacturing of Skins Based on Composite Corrugated Laminates for Morphing Aerodynamic Surfaces
Smart Materials and Structures, Vol. 26, N. 4, 2017, 045024 (22 pages)
doi:10.1088/1361-665X/aa6069

Design and manufacturing of skins based on composite corrugated laminates for morphing aerodynamic surfaces

Alessandro Airoldi[1*], Stephane Fournier[1], Elena Borlandelli[1], P. Bettini[1] and G. Sala[1]
[1]Dept. of Aerospace Science and Technology, Politecnico di Milano
Via La Masa, 34 – 20156 Milano – Italy

*Corresponding author: alessandro.airoldi@polimi.it

Abstract

The paper discusses the approaches for the design and manufacturing of morphing skins based on square-shaped composite corrugated laminates and proposes a novel solution to integrate in the skin an elastomeric cover to prevent detrimental effects of corrugation on aerodynamic performances. Additionally, more complex corrugated shapes are presented and analysed. Design and manufacturing issues related to the production of corrugated laminates are discussed in detail, considering stiffness requirements derived from previously performed aeroelastic analyses of a morphing concept. A solution is proposed to integrate an elastomeric cover in the corrugated skin and a manufacturing process is presented and assessed. Moreover, a fully non-linear numerical model is developed and characterized to study the behaviour of this skin concept in different load conditions. Finally, configurations based on combination of square-shaped corrugated panels are considered. Their structural properties are numerically investigated by varying geometrical parameters. Performance indices are defined to compare structural stiffness contributions in non-morphing directions with the ones of conventional panels of the same weight. The overall results validate the design approaches and manufacturing processes to produce corrugated laminates and indicate that the solution for the integration of an elastomeric cover is a feasible and promising method to enhance the aerodynamic efficiency of corrugated skins. Numerical studies

also show that the extension of the concept to complex corrugated shapes may improve both the design flexibility and some specific performances with respect to simple corrugations.

1. Introduction

Structures capable of a smooth and progressive shape change without experiencing damage or permanent deformations can provide novel solutions for the generation of aerodynamic forces required to guide, control and stabilize aerospace vehicles as well as to optimize them for different missions or mission segments. Such type of structures, which are currently referred to as morphing structures, can perform with more efficiency and versatility the functions of the rigid moveable aerodynamic surfaces, such as flaps and ailerons, which are conventionally adopted in the aerospace field. In recent years, researchers have devised and analysed a large variety of morphing solutions, sometimes inspired by biomimesis or conceived by exploiting the properties of advanced materials and actuation concepts [1,2].

Generally, the design of a morphing structure represents a challenging task for engineers, since the desired progressive shape change requires tuneable compliance and high deformability in well-defined directions, which can be defined as morphing directions, but, at the same time, significant load carrying capability and stiffness should be retained in other directions. A typical case is represented by the skin of morphing structures, which should undergo to large deformations required by shape changes without damages but is also required to collect aerodynamic pressures and transfer their resultant to the main structure without excessive local waviness. Functional requirements for such flexible skins actually depend on the specific performance and working conditions. In the cases presented in [3], requirements in morphing direction are the capability of undergoing large recoverable strains, with a low axial compliance in order to reduce the forces needed for actuation and a sufficient bending stiffness to avoid skin bubbling or instability. However, different applications can specifically require low bending stiffness and no axial compliance, such as in the case of the morphing leading edge presented in [4,5].

Moreover, considering the role of the skin in conventional aircraft stressed-skin constructions, an optimal solution should also provide a contribution to carry shear and normal loads in non-morphing directions, in order to reduce the weight cost related to morphing. Since the skin represents a fundamental

ingredient of all the types of morphing aerospace structures, the identification of an adequate design concept is of paramount importance for the successful implementation of morphing solutions.

Corrugated panels represent a particularly appealing concept to accomplish the aforementioned conflicting requirements, since they can be easily extended and bended along the direction of the corrugated profile and exhibit high stiffness and strength properties normally to the corrugate profile. Production of corrugated sheet by lamination of composite plies enhances the design flexibility of this structural concept, because the degree of structural anisotropy can be increased by selecting the most convenient lay-ups. Usage of composite corrugated laminates for morphing skins was proposed in [6] and their potential was recognized very soon [7, 8]. Morphing solutions based on corrugated composite laminates were manufactured and their aerodynamic performance were tested and analysed by using Computational Fluid Dynamic models in several works [9-11].

The interest in corrugated laminates for morphing has promoted the development of approaches to evaluate the stiffness properties of different corrugated geometries, made of circular segments or having trapezoidal and rectangular shapes with rounded angles, as, for example, in [6, 12, 13]. According to [14], maximum and minimum stiffness levels, for a given set of geometrical and material properties, can be obtained by considering two limiting geometries, namely a triangular and a trapezoidal shape. Analytical models were also developed by different authors to derive the properties of homogenized orthotropic plate models. Such homogenized models can be used to effectively model morphing aircraft components at the structural scale level, as it was done in [15, 16]. A detailed comparison between analytical predictions, finite element models and experiments was presented in [13]. The homogenization technique proposed by [17] can be considered an extension of the analytical models and can be adopted to obtain the complete stiffness matrix for a generic corrugated shape, although a finite element approach could be required in the case of thick or asymmetric laminates [18]. Recently, the properties of more complex corrugated geometries made of composite laminates have been analysed to enhance design flexibility of the concept [19, 20].

Although corrugated laminates can be designed to meet highly demanding requirements in morphing and non-morphing directions, a fundamental issue is represented by alterations induced in the lift curve and in the drag coefficient of an airfoil endowed with a corrugated skin, when the flow is parallel to

morphing direction. Such issue had already been considered in [6], and the proposed solution consisted in filling the valleys of the corrugation with an elastomer. The problem was more accurately analysed in [10], showing that detrimental effects due to corrugation can be reduced at an acceptable level by limiting the corrugation depth to less than 1% of the profile chord. A discontinuous segmented skin was suggested and used in experimental tests to improve aerodynamic performances [9]. A detailed investigation of corrugation effects has been presented in a more recent work [21], where high reductions of the lift to drag ratio were found with respect to the one of a smooth airfoil with a corrugation depth equal to 1% of the chord. Such observations clearly indicate that the advantages obtained by the adoption of a seamless and adaptable morphing profile with a corrugated skin could vanish considering the reduction of aerodynamic performances.

The main objective of the paper is the development of morphing skin concepts based on corrugated laminates that can fulfil realistic aeroelastic requirements, prevent detrimental effects of corrugation on aerodynamic performances and provide adequate structural contributions in non-morphing directions.

To accomplish such goals, design approaches and a technological process are first presented, aiming at manufacturing composite corrugated laminates with a square-shaped corrugation designed to meet the requirements derived from an aeroelastic optimization process, carried out in a previous work [15]. In a subsequent section, an efficient and lightweight solution is presented to address the aerodynamic issues related to corrugation effects. The integration of an elastomeric cover in the square-shaped corrugated laminate, supported by honeycomb stripes is described and the manufacturing process is assessed. Moreover, this section includes tests and numerical evaluations to show that the external cover does not interfere with the compliance of the corrugated support and that it minimizes the waviness of the external surface under different combinations of applied pressures and morphing deformation. A further section is aimed at extending the concept of corrugated supports for morphing skin to more complex configurations, which can be manufactured by combining square-shaped corrugated laminates. Performance indices are defined and applied to investigate responses in morphing and non-morphing directions. Parametric studies are carried out to evaluate the effects of the most significant geometric design variables and to compare simple and complex types of corrugation. In particular, bending stiffness in non-morphing direction and in-plane shear stiffness are compared to the ones achieved by a conventional flat panel,

with no morphing capabilities, having the same weight of the morphing panel. The most important findings of the research activity are summarized in a final section.

2. Design and manufacturing of corrugated panels with square-shaped profile

2.1 Formulations for the design of a corrugated composite panel

Axial and bending stiffness levels required to a morphing skin, in the morphing direction, depend on a large number of factors, including operative working conditions, constructive constraints, and structural functions performed by the aerodynamic surface. The evaluation of the requirements may be carried out by considering the panel as generic orthotropic plate, with the following stiffness matrix:

$$\begin{Bmatrix} \mathbf{N} \\ \mathbf{M} \end{Bmatrix} = \begin{bmatrix} \overline{\mathbf{A}} & \overline{\mathbf{B}} \\ \overline{\mathbf{B}}^T & \overline{\mathbf{D}} \end{bmatrix} \begin{Bmatrix} \boldsymbol{\varepsilon}_0 \\ \boldsymbol{\kappa} \end{Bmatrix} \tag{1}$$

where **N**, **M** are the membrane forces and bending moment per unit width applied to the corrugated laminate, whereas $\boldsymbol{\varepsilon}_0$ and $\boldsymbol{\kappa}$ are the deformations and the curvatures of its mid-plane. The terms $\overline{A}_{ij}$ and $\overline{D}_{ij}$ represent the membrane and bending stiffness properties of the corrugated, which are homogenized into the ones of the equivalent orthotropic panel. In the paper, axis 1 is taken along the corrugated profile, that is in the morphing direction , whereas axis 2 indicates the transversal, non-morphing direction. The approach based on the homogenization can be efficiently used in aeroelastic models to identify the requirements for a skin in a specific morphing solution.

An example is provided in [15], where an optimization process was performed by using a numerical aeroelastic model of an airfoil with the capability of varying camber under the action of aerodynamic loads. Additional details on the internal flexible structure of the proposed morphing solution are presented in [16], whereas the present work analyses the requirements for the skin and discuss the selected solutions.

The profile considered in [15] had a chord of 1 m and its performance were investigated at an airspeed of 42 ms^{-1}. The properties in the morphing direction were included in the set of problem design variables.

Results indicated that a low membrane axial stiffness, $\overline{A}_{11} < 30$ Nmm^{-1}, is suited for the morphing performance and does not affect the capability of the skin to collect the aerodynamic pressure. However, bending stiffness, $\overline{D}_{11}$, had to be kept beyond a threshold, 500 Nmm ÷ 600 Nmm, in order to avoid bubbling, which originated oscillations in the distribution of pressure coefficient on the wing surface. Hence, results confirmed the main findings in [3] and are used in this work as a reference to present the basic issues regarding the design and the production of a composite corrugated panel.

The identification of an engineering solution requires prediction tools to evaluate the homogenized properties that can be obtained by a corrugated composite laminate with a given set of geometrical parameters, material properties and lay-up.

Indeed, corrugated panel can be shaped according to different geometries, such as in the examples provided in figure 1-(a) and 1-(b), referred to a curved corrugated shapes, originally proposed in [6] and the square-shaped one, respectively. Such square-shaped geometry actually includes rounded fillets, which must be introduced to obtain technologically feasible configurations.

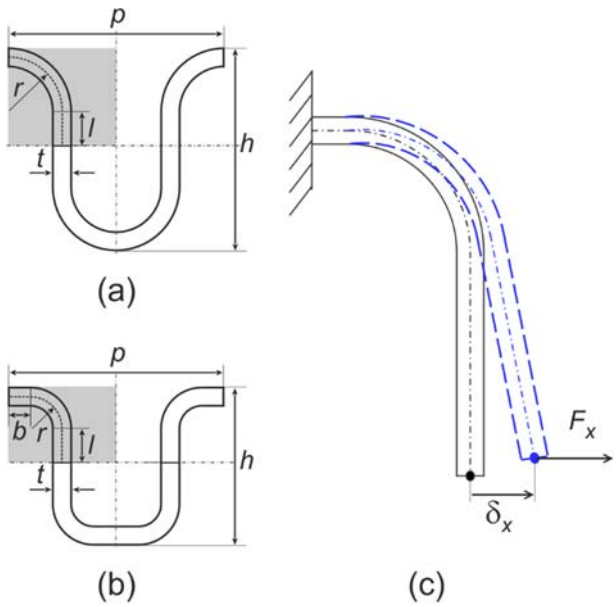

Figure 1. Rounded (a) and square-shape (b) corrugations, and scheme for the evaluation of properties in morphing direction (c).

Several general formulations exist to calculate all the stiffness properties of homogenized panels [17, 18]. Most of them are based on the application of Euler-Bernoulli or thin shell theory. An extension of

such theories is hereby proposed to consider transverse shear deformation in the laminate. Accordingly, axial and bending stiffness in the morphing direction for the shapes presented in figure 1-(a) and figure 1-(b) were obtained by applying Timoshenko beam theory. The unit element represented in figure 1-(c) was considered, which represents an horizontal curved and vertical part of the corrugated panel considered in cylindrical bending (i.e. without displacement or force gradients along the panel width). The differential equations that derive from the application of Timoshenko beam theory are reported in Appendix A. They lead to the expressions reported in (2), which can be considered an extension of the Euler-Bernoulli formulations presented in [17]. Although such expressions were obtained for the square-shape corrugation presented in figure 1-(b), they are also valid for the round-shaped type of figure 1-(a), if the length of the horizontal arm, *b*, is set to zero.

$$\begin{aligned} \overline{A}_{11} &= \frac{4(r+b)}{\left[\dfrac{Q_1}{A_{11}} + \dfrac{Q_2}{D_{11}} + \dfrac{Q_3}{(kGt)_{eq}}\right]} \\ \overline{D}_{11} &= \frac{r+b}{\dfrac{\pi}{2}r + l + b} D_{11} \end{aligned} \tag{2}$$

A_{11} and D_{11} in (2) are the terms of the stiffness matrix of the composite plate that is laminated according to the corrugated shape, and $(kGt)_{eq}$ is the equivalent transverse shear stiffness per unit width. The coefficients Q_1, Q_2 and Q_3 have the following expressions:

$$\begin{aligned} Q_1 &= \pi r - 4b = I_1 \\ Q_2 &= 4l^2\left(b + \frac{l}{3}\right) + 2rl(4b + \pi l) + r^2(4b + 8l + \pi r) = I_2 \\ Q_3 &= \pi r + 4l = I_3 \end{aligned} \tag{3}$$

Considering the bending stiffness term, $\overline{D}_{11}$,the formulation reported in [6] for the rounded geometries turns out to be identical to the one reported in (2) and (3), if $b = 0$ is assumed. Considering the formulation for the axial stiffness, the expression provided in (2), obtained by applying Timoshenko Beam Theory (TBT), can be transformed in the expressions obtained in [6] and in [17], by changing the values of the coefficient Q_j, according to indications reported in table 1.

Table 1. Coefficients in the expression of axial stiffness according to different formulations.

	Yokozeki et al.	Xia et al.	TBT
Q_1	*0*	I_1	I_1
Q_2	I_2	I_2	I_2
Q_3	*0*	*0*	I_3

The analytical formulations expressed in (2) and (3) were applied to try to identify a composite corrugated panel fulfilling the requirements $\overline{A}_{11} < 30$ Nmm^{-1} and 500 Nmm $< \overline{D}_{11} < 600$ Nmm, obtained in [15]. An homogeneous $[0]_n$ lay-up was considered for the corrugated panels. Selected material was SEAL CC90/ET443 carbon/epoxy fabric, with the properties reported in table 2. Moreover, technological limitations regarding the minimum radius, *r* were taken into consideration to select a feasible configuration.

Table 2. Properties of composite plies used in the design of the corrugated panel

$E_{11} = E_{22}$	MPa	56550
ν_{21}	-	0.05
G_{12}	MPa	4040
$G_{13} = G_{23}$	MPa	3000
ply thickness	mm	0.113

A set of technologically feasible solutions were obtained by adopting a period, *p*, of 24 mm and a minimum fillet radius, *r*, of 2 mm. The stiffness parameters of the identified design hypotheses are reported in table 3. It can also be observed that, in the considered case, the different analytical formulations for the evaluation of the axial stiffness provide almost identical results.

The round-shaped corrugation almost meets the requirements by using the geometrical parameters in table 3 and a number of plies, *n*, equal to 5, although bending stiffness is underestimated. For a square-shaped corrugation with the same overall height and pitch, the bending stiffness turns out to be slightly lower the required limit with *n*=5. However, if the number of plies is increased to 6, both axial and bending stiffness are slightly beyond the desirable limits.

Table 3. Design hypothesis for the corrugated skin

Type	r (mm)	L (mm)	b (mm)	n plies (-)	$\overline{A}_{11}$ Yokozeky et al. (Nmm^{-1})	$\overline{A}_{11}$ Xia et al. (Nmm^{-1})	$\overline{A}_{11}$ TBT (Nmm^{-1})	$\overline{D}_{11}$ (Nmm)
Round	6.0	1.0	0.0	5	20.34	20.33	20.12	490.42
Square	2.0	4.0	4.0	5	N/A	20.14	19.95	458.87
Square	2.0	4.0	4.0	6	N/A	34.81	34.32	792.92

In this work, the solution with the square corrugation was selected to manufacture a prototype of the skin system. One of the fundamental reasons for such a choice was the need of a horizontal surface to provide the support for the elastomeric cover. The integration of such cover in the square-shaped corrugated laminate will be presented in section 3.

2.2 Manufacturing of square-shaped composite corrugated laminates

Production of thin corrugated composite laminates, with good manufacturing quality, involves some technological issues. Actually, difficulties for manufacturing corrugated composite panels depend on the shape of the corrugation, since lamination of deeply corrugated shapes and presence of fillets with small radii significantly complicate the process.

The need for a step-by-step lamination procedure to force the pre-preg plies into a corrugated metallic mould was outlined in [9]. In such work, the lay-up was kept in position by the application of metallic bars during lamination. The methodology for the production of rounded corrugation shape described in [22] was based on application of a metallic mould, but authors' findings indicate that the adoption of a metallic counter-mould turns out to significantly improve the quality of the laminate and the consequent strength properties.

In the present work, a light alloy mould was machined to obtain a square-shaped corrugated panel with the geometrical characteristics reported in table 3. Initially, technological trials carried out by considering a lamination sequence $[0]_3$. The layers were individually laid on the mould by using a heat gun to facilitate forming. Three corrugated samples with a width of 140 mm and a total length of 280 mm (including 12 unit cells and two flat ends for the insertion into test machine grips) were produced by using the mould shown in figure 2. Manufacturing was carried out both the application of a metallic

counter-mould and of an elastomeric counter-mould, which was produced by using a non-siliconic elastomer (Airpad^{TM}), having a use temperature higher than 200°C. The elastomeric counter-mould was shaped at 176 °C in autoclave by using the same mould prepared for the corrugated panel. The quality of the laminates obtained the metallic and the elastomeric counter-mould is presented in figure 3. Several voids and surface defects are apparent in the corrugated panel shown in figure 3-(a), particularly in the fillets. Such panel was produced with the metallic counter-mould and can be compared with the one presented in figure 3-(b), which was produced by using the elastomeric counter-mould and presents an appreciable surface finishing.

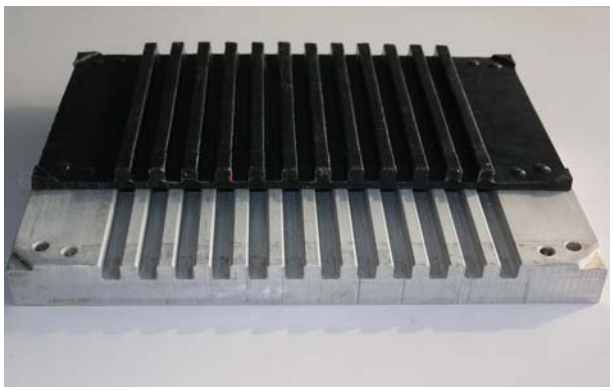

Figure 2. Mould and elastomeric counter-mould used for corrugated panel production

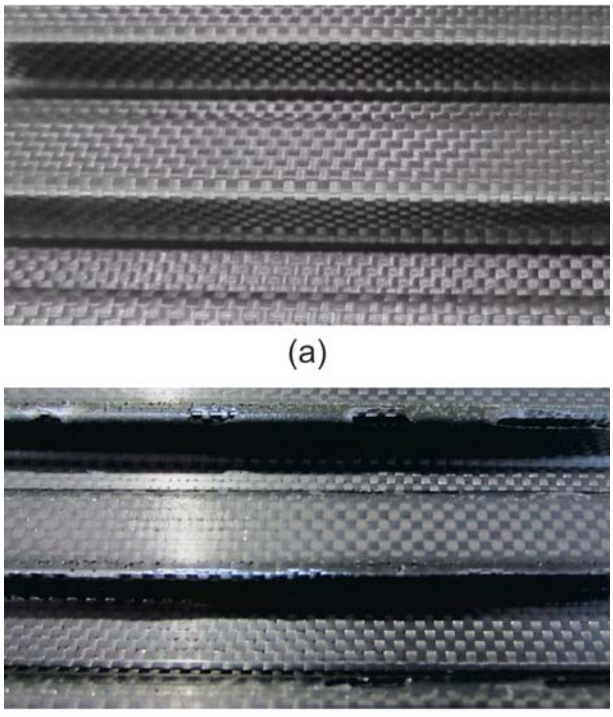

Figure 3. Surface of the corrugated panels produced with a metallic (a) and an elastomeric counter-mould (b)

Tensile tests were carried out on the specimens produced. The experimental set-up is shown in figure 4-(a), and the results of the tests are presented in figure 4-(b). It can be observed that the two tests performed on the panels manufactured with the elastomeric counter-mould are characterized by a lower stiffness, but presents higher displacement at failure and maximum load than the coupon produced with the metallic counter-mould. The difference in stiffness is due to a different compaction of the plies, which leads to a slightly lower thickness in the laminates produced with the elastomeric counter-mould, whereas the improvement in ultimate load and displacement indicates the improved quality of the laminate.

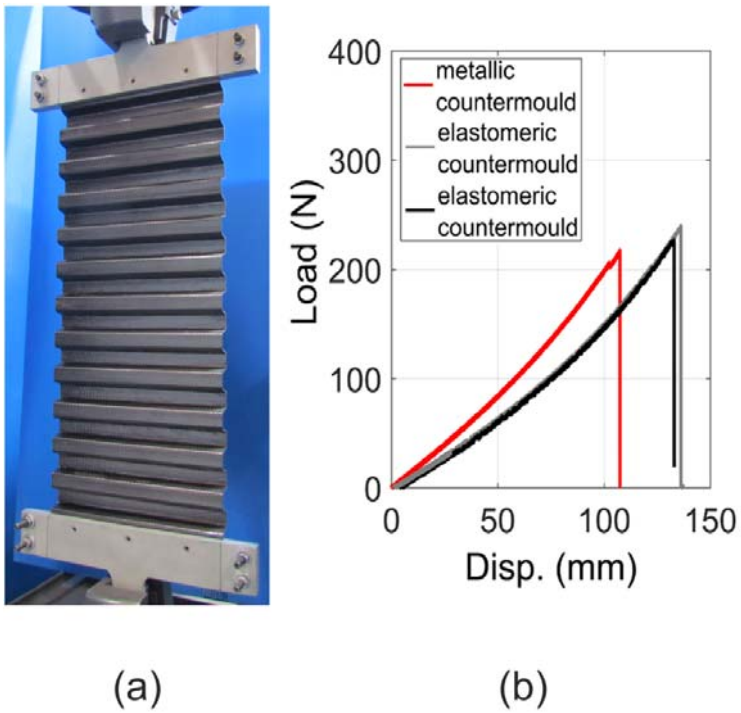

Figure 4. Experimental procedure (a) and results (b) of the tests on corrugated panels

2.3 Testing and modelling of corrugated laminates based on square-shaped cell

On the basis of the results of the technological trials, corrugated panels were produced by using the mould and the elastomeric counter-mould shown in figure 2 and adopting a $[0]_5$ lamination sequence, which was considered acceptable for the requirements provided in [15] for the skin, according to the results in table 3.

The development of a technology to produce square-shaped corrugated laminate also provided the opportunity to explore combined corrugated shapes. For instance, a corrugated panel made of a sequence of deformable and closed square cells was obtained by bonding together two corrugated laminates, as it

is exemplified in figure 5-(a). Indeed, a similar geometry, which will be referred to as twin corrugated laminate, was used in [9]. Properties of configurations with closed shells, based on square-shaped corrugated laminates will be evaluated and compared with simply corrugated laminates in section 4 of this paper.

A twin corrugated panel is shown in figure 5-(a). Bonding between the two simply corrugated laminate was carried out by means of stripes of adhesive film 3M AFK-163-2K, which were set on the adjacent horizontal parts and cured in a secondary process by using a heated plate press

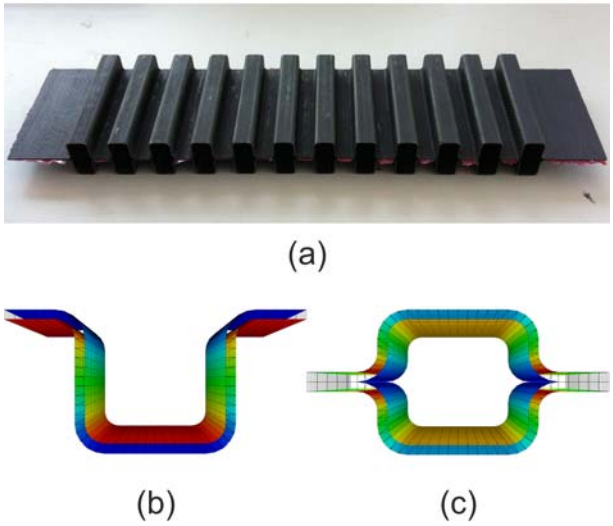

Figure 5. Manufactured twin corrugated panel (a) and FE model of a simple corrugated (b), and twin corrugated laminate (c)

All panels had a width of 140 mm and a total length of 280 mm, with 12 unit cells. They were tested in tension by adopting the same test lay-out shown in figure 4-(a). Two finite element models of the unit cells referred to both the corrugated laminates were developed and solved by using Abaqus/Standard FE code. Panels were modelled by using 8-noded continuous shells (*Elements SC8R* [23]), which have the behaviour of conventional thick shell elements but represent the physical geometry of the laminate in the in-plane and trough-the-thickness direction. The models are shown in figure 5-(b) and figure 5-(c) for the simple and the twin corrugated laminate, respectively. Linear and geometrically non-linear analyses were conducted by using the Abaqus/Standard code, by constraining the rotations at the end of the cell and applying an axial displacement. Such conditions were enforced to represent a test performed on a periodic corrugated structure. The results are shown in figure 6, in terms of axial force per unit with, $N_{x,}$ vs. the mid-plain engineering strain ε_0. Analytical models of the simple corrugated laminate are also

included in the comparison presented in figure 6, which reports the force per unit width at ε_0 = 0.1 calculated by applying the stiffness predicted in table 3.

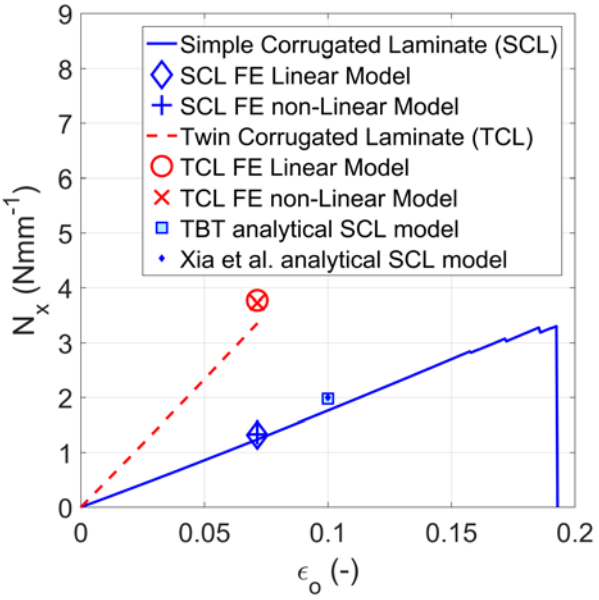

Figure 6. Experimental, numerical and analytical axial response of simple and twin corrugated laminates

The results indicate that the axial compliance of the simple corrugated laminate is about three times the one of the twin corrugated laminate. Strains at failure can not be compared, since the twin corrugated laminate was not brought to failure in the experiments. The numerical-experimental correlation indicates that the finite models developed can obtain an acceptable correlation with the experimental stiffness of the corrugated panels, although an error of 10% is obtained considering the double corrugated case. Analogously, analytical predictions for single corrugated laminates are in acceptable agreement with experiments, although the analytical stiffness is slightly overestimated. Such errors are likely to be originated by discrepancies between nominal and cured ply thickness as well as by geometrical imperfections and by difficulties in accurately modelling the extension of the bonded zone , in the twin corrugated laminate.

3. Integration of an elastomeric cover in the morphing skin

3.1 Development of a technological solution

A fundamental problem for the development of morphing skins based on corrugated laminates is represented by the effect of corrugation on aerodynamic performance. According to numerical and experimental analyses, airfoils endowed with corrugated trailing edges present significant increase of drags and a reduced slope of lift vs. angle of attack curve with respect to conventional airfoils with smooth skins [10, 11]. Indeed, problems originated by waviness of the aerodynamic surface had been already considered in [6], where it was proposed to fill the “valleys” of the corrugation by using elastomeric material. However, such solution can result in significant additional weight, particularly for deeply corrugated shapes. A different strategy was adopted in [9], where an externally segmented composite skin was bonded to the corrugated laminate to improve aerodynamic performances in wind tunnel tests. In such solution, small strips of composite laminates, bonded at one end, cover the “valleys” of the corrugation. Such segmented skin can reduce the detrimental effects of corrugation on the aerodynamic performances, but, in real world applications, the presence of platelets bonded to surfaces is likely to present some drawbacks concerning structural integrity, aerodynamic efficiency, vibrations and limited applicability in the case of large curvatures.

An alternative, efficient and lightweight solution is hereby proposed based on an elastomeric external cover that is sustained, in the “valleys” of the corrugation, by strips of conventional hexagonal-cell honeycomb, with cell axes directed perpendicular to the cover. In the solution, which is sketched in figure 7-(a), the elastomeric cover is bonded on the horizontal arms of the corrugation. The honeycomb should only provide a support to the elastomer in the vertical direction, with a minimal interference on the overall deformation mechanism. Such goal could be accomplished thanks to the significant orthotropy of honeycomb and, particularly, to the very low stiffness properties in the plane of the hexagonal cells.

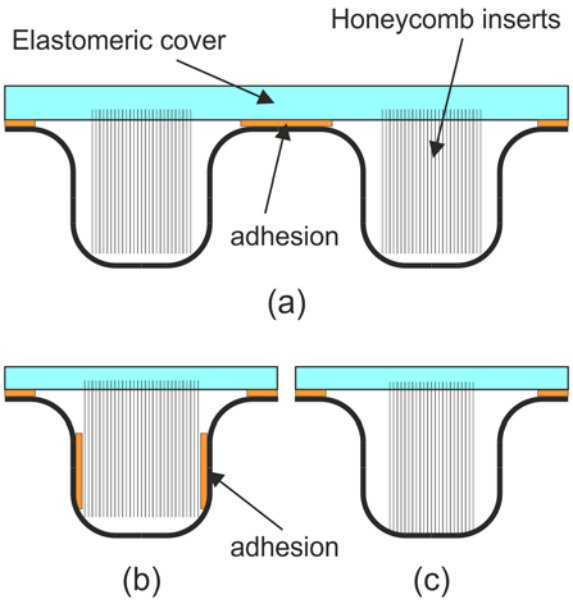

Figure 7. General lay-out of the skin system (a) and configurations with honeycomb lateral surfaces bonded (b) and non-bonded (c) to corrugated laminate

The concept presented in figure 7-(a) was considered to manufacture a 280 mm long, 140 mm wide skin panels, by using the simply corrugated laminates described in section 2.2. Honeycomb stripes with a height of 12 mm and a width of 12 mm were cut from a sheet of Hexcel™ HRH-10 aramid honeycomb, with a density of 48 kg/m^3 and a cell size of 3 mm. The elastomeric cover was obtained by using a a siliconic rubber (RECKLI^{TM} SI compound 6.25) with a shore hardness of approximately 25.

The integration of honeycomb stripes and of the elastomeric cover was performed in a secondary technological step, after the production of the composite corrugated laminate.

Initially, the configuration presented in figure 7-(b) was considered, where honeycomb lateral surfaces are bonded to the vertical arms of the corrugated laminate, to support the elastomeric cover. In a manufacturing trial, honeycomb was bonded inside the valleys of the corrugated laminate and then tested without the application of the elastomeric cover. Bonding was obtained by applying a film of 3M AFK-163-2K adhesive to the lateral surface of the honeycomb stripes. The stripes were inserted in the corrugated laminates and vacuum assisted curing was performed in an oven, at a temperature of 120° C. A detail of the obtained panel is shown in figure 8-(a). The panel was tested by using an Instron 4302

electromechanical test system. The panel ends were gripped into metallic plates as shown in figure 8-(b). The obtained response, presented in figure 8-(c), was characterised by an initial stiffness $\overline{A}_{11}$ = 102 Nmm^{-1}, which is significantly higher than the values of about 20 Nmm^{-1} provided by the analytical predictions, presented in table 3 for the composite corrugated laminate alone. Moreover, a premature failure was achieved, at a displacement corresponding to a strain level of about 1.6%. Such failure was due to the debonding of a honeycomb stripe and was followed by subsequent failures of all the other bonding lines. Subsequent failures originated a segmented force vs. displacement response, shown in figure 8-(c). The test was continued until the final failure of corrugated laminate, which occurred at a displacement corresponding to strain level of 18.5%.

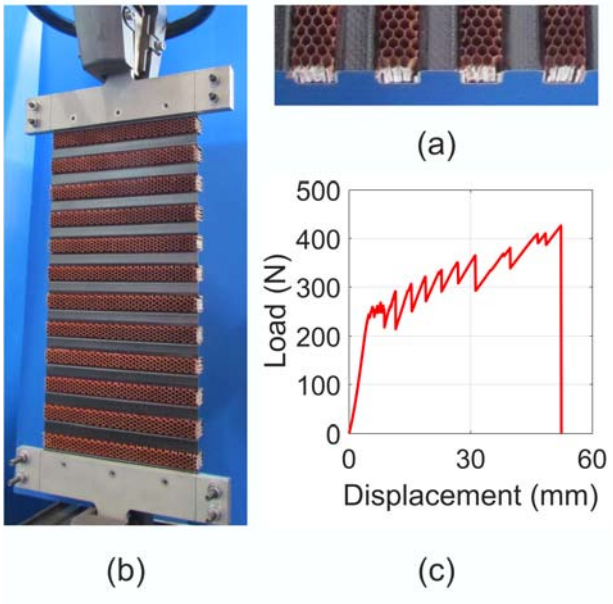

Figure 8. Detail of honeycomb integration (a), lay-out of testing test (b) and force vs. displacement response (c)

The results obtained in this first integration test demonstrated that bonding of honeycomb lateral surfaces to the corrugated laminate significantly influences the overall deformation mechanism. Indeed, the vertical arms of the corrugated laminate undergo flexure so that the axes of the honeycomb cells bonded to them are required to bend when the system is stretched. Bending of cell axes involves axial strain of cell walls in the direction parallel to cell axes, and originates not negligible stress levels. Consequently, the overall stiffness of the laminate is noticeably increased.

Moving from such results and considerations, direct adhesion between honeycomb surfaces and corrugated laminate was eliminated in the final version of the skin. Application of honeycomb was obtained by integrating the stripes into the elastomeric layer during vulcanisation, and supporting function was obtained by allowing a contact between the lower surface of the honeycomb stripe and the horizontal arm of the corrugated laminate, as it is sketched in figure 7-(c). The technological process to manufacture such skin system made use of the same mould adopted for the production of the corrugated laminated, which was used to house the laminate and to keep in position the honeycomb stripes as indicated in figure 9-(a). The surface of the upper horizontal arms was treated with a specific primer (RECKLI Primer SI) to guarantee adhesion with the elastomeric cover. The mould was then capsized and introduced into a container filled with a layer of liquid elastomer mixed with the vulcanization agent. During vulcanization, which takes several hours, the liquid silicon rubber penetrated by capillarity into the honeycomb cells. At the same time, adhesion between the horizontal arms and the elastomeric cover was obtained thank to surface treatment, as prescribed in figure 8-(a). A detail of the result is shown in figure 9-(b), whereas figure 9-(c) is referred to the tensile test performed on the final skin system.

The result of this test is provided in figure 10. The response of the corrugated laminate without any additional feature is also presented and compared with the results of the configuration sketeched in figure 7-(b), reproduced from the data already presented in figure 8-(c). Such comparison confirms the undesired stiffening effect of lateral honeycomb bonding in the first configuration tested, which actually increased the panel stiffness until the failure of all the lateral bonding lines. Indeed, it can be seen that when all the bonding lines are failed, the secant stiffness turns out to be similar to the original one of the corrugated laminate. Analytical predictions, evaluated for the panels from the values in table 3, are also reported in figure 7. Considering the final version of the skin system, with honeycomb stripes integrated in the elastomeric cover, the response is very closed to the one of the corrugated laminate alone. Accordingly, the integration of the elastomeric cover, supported by the honeycomb to obtain a smooth aerodynamic surface, did not affected the tensile stiffness of the system. The slight progressive reduction of the stiffness observed in the experimental test can be attributed to the slipping of the silicon elastomer between the metallic plates applied to grip the specimen during the test.

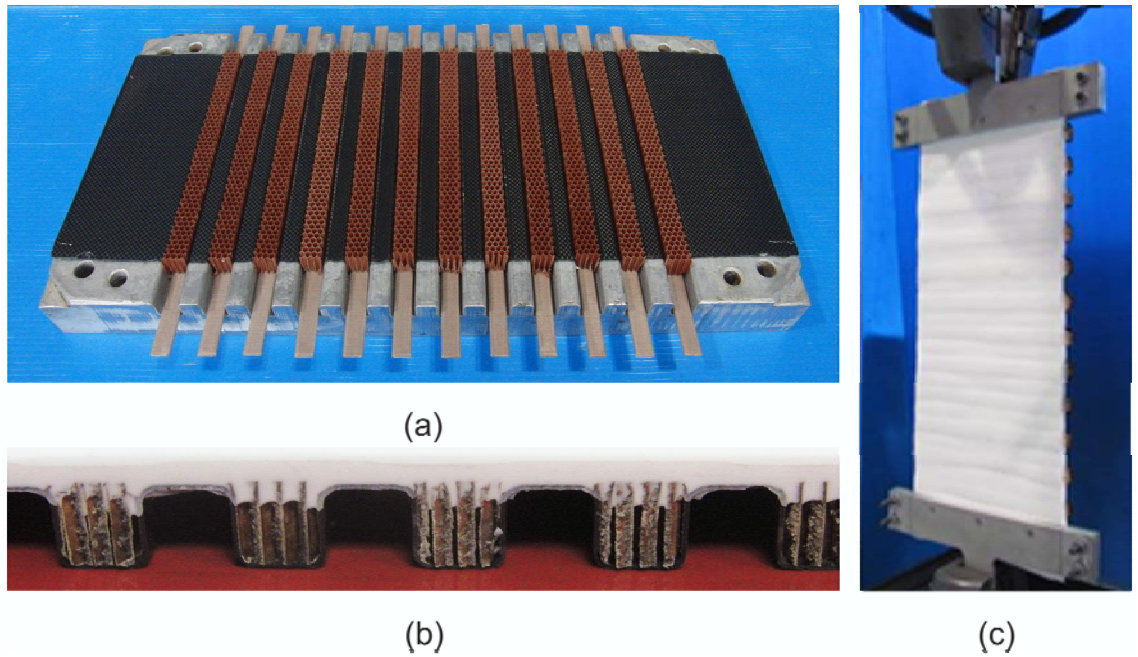

Figure 9. Positioning of honeycomb stripes into the corrugated laminate (a), integration of elastomeric cover (b) and test on the final skin system (c)

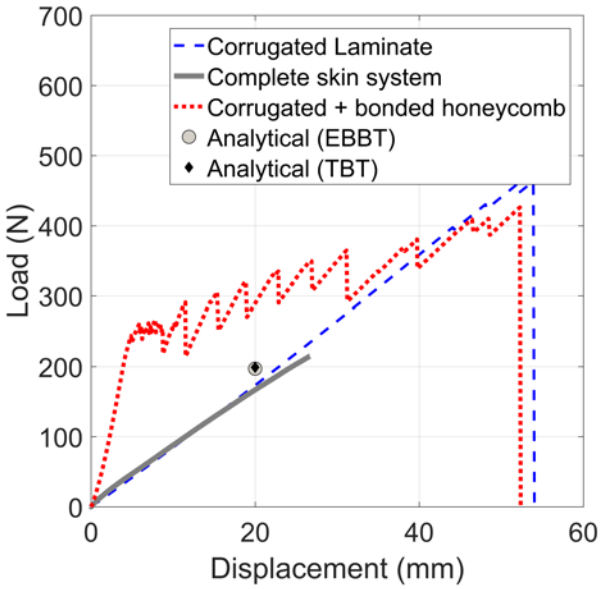

Figure 10. Result of tensile tests performed on corrugated laminates and on complete skin system

3.2 *Material characterisation for a detailed model of the skin system*

Results obtained for the integration of the elastomeric cover into the corrugated laminate are promising to develop a structurally and aerodynamically efficient morphing surface. However, even such technological solution can not guarantee a perfectly smooth surface, as it can be noticed in the picture presented

in figure 9-(c), since the elastomeric cover assumes a deformation characterized by bands with different surface displacements, originated by the different type of internal support provided by the composite laminate and the honeycomb stripes.

To evaluate the surface waviness under different operative conditions, a detailed non-linear finite element model was developed and analyzed. Analyses were carried out considering different tensile and compressive axial loading and the action of aerodynamic pressure.

An accurate characterization of the hyper-elastic response of silicon elastomer was considered important to obtain reliable numerical results. Tension tests were performed on two types of specimens, to obtain the silicon elastomer response in two different stress states. Such tests, which are described with more detail in Appendix B, were used to characterize a hyperelastic material model by using the second order form of the Odgen strain energy potential [24], reported in (4).

$$U=\sum_{i=1}^{2}\frac{2\mu_i}{\alpha_i^2}\left(\overline{\lambda_1}^{\alpha_i}+\overline{\lambda_2}^{\alpha_i}+\overline{\lambda_3}^{\alpha_i}-3\right)+\sum_{i=1}^{2}\frac{1}{D_i}\left(J^{el}-1\right)^{2i} \tag{4}$$

where J is the volumetric deformation, $\overline{\lambda_1}=J^{-1/3}\lambda_1$ are the normalized form of the principal stretches of the deviatioric tensor, λ_i. Material parameters μ_i, α_i, and D are found by minimizing the discrepancies between the experimental and the numerical response in both uniaxial and planar test. Such identification process is actually a built-in procedure in the Simulia/Abaqus code [23] and provided the values given in table 4.

Table 4. Material model parameters of elastomeric material

	μ	α	D
i = 1	$7.15\cdot10^{-2}$	3.07	0.46
i = 2	$-1.54\cdot10^{-2}$	-5.67	0

For the honeycomb material, a linear elastic orthotropic material was selected, with axis 3 along the cell axes and axes 1 and 2 in the plane of the cells. The most significant stiffness constants, in the out-of-plane direction, were obtained from the producer datasheet and were integrated by assuming an isotropic

behavior in the plane of the cells, with very low elastic moduli E_{11} = E_{22} = 0.01 MPa and a Poisson's ratio v_{12} of 0.3. The in-plane shear modulus turns out to be G_{12} = 0.0038 MPa, from isotropic assumption. Properties in the out-of-plane direction are E_{33} = 138 MPa, G_{13} = 40 MPa and G_{23} = 25 MPa. The Poisson's ratios v_{13} and v_{23} were set to 0.001.

3.3 Numerical analysis of surface smoothness in different operative conditions

A fully non-linear model of a 50 mm wide, two-cell chunk of a corrugated laminate, with a $[0]_5$ lay-up and geometrical parameters defined in table 3, was developed, including the honeycomb and the elastomeric cover. In the model, presented in figure 11, the elastomeric cover and the honeycomb inserts were modelled by using solid elements with sizes ranging from 0.5 mm to 0.8 mm, characterized by the previously described material models. The corrugated composite laminate is represented by shell elements with a typical size of 1 mm, which are rendered with their thickness in the visualization presented in figure 11-(b) and figure 11-(c), to show the contact interaction between the honeycomb and the composite laminate.

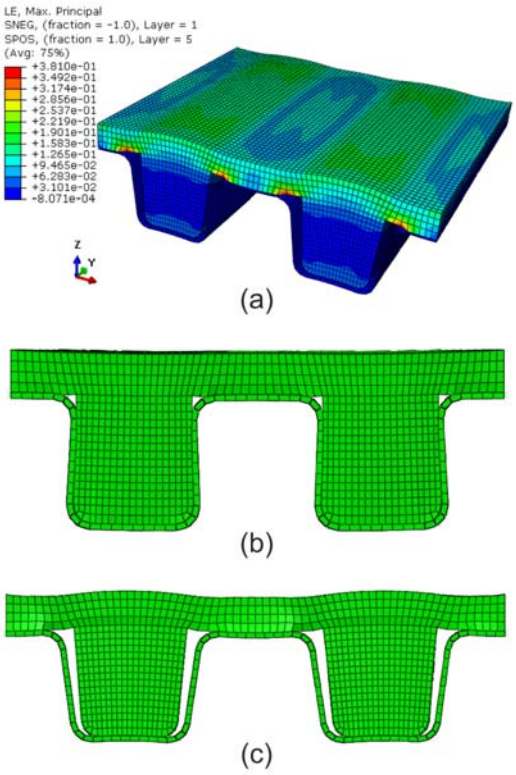

Figure 11. Detailed non-linear finite element model of the skin system: contour of strain in tensile analyses (a), deformed shape in tensile (b), and compressive analyses with pressure (c)

The adhesion between the elastomeric layer and the horizontal upper arm of the composite laminate was modelled by using an algorithm available to join dissimilar meshes in the solver code (*Tie Algorithm* [23]), whereas a contact interaction, with a friction coefficient of 0.9, was set between the side of the honeycomb stripes and the internal surface of the composite laminate.

The model was used to analyze the smoothness of the surface in the proposed skin system, under the action of the aerodynamic pressure and in different tension and compression conditions. Hence, the objective of the numerical activity was a quantification of the waviness that has to be expected if the proposed design solution is adopted. Although analyses are referred to specific configurations and design conditions, the indications regarding the performances and the methodological approach have a more general validity.

Numerical analyses were performed by applying a displacement corresponding to a stretching of about 12% in tension and compression direction. In the same analyses, increasing pressures were applied to the external surface of the elastomeric layer, taking as a reference a pressure $p_{ref} =$ 0.018 MPa, which is the maximum aerodynamic pressure achieved in the design conditions considered in [15], at an airflow speed of 41 m/s. The model, which represents two unit cells for a total length of 48 mm, was supported in the vertical direction at both ends. Moreover, an identical displacement was imposed to all of the nodes at the ends, in order to achieve the desired stretching levels. Accordingly, no rotation at the end was possible.

The length of the model in the morphing direction, corresponding to two periods, is consistent with the distance between the skin supports in the morphing airfoil that was taken as a reference in this work [15, 16]. Indeed, the space interval between the vertical supports greatly influences the total deflection. For such a reason, it was decided to separately consider the overall bending deflection of the skin, considered as a homogenized plate, from the local waviness of the external surface. This choice is motivated by the fact that limitation to the overall bending deflection is already taken in consideration in aeroelastic analyses, where the skin is represented at the homogenized level. Accordingly, overall bending deflection has to be controlled by properly choosing material, geometry and lay-up of the corrugated profile,

whereas the analyses performed with the detailed non-linear model have to focus on local waviness of the external surface. To separate the displacements due to global bending from local waviness, vertical displacements due to overall bending response were estimated through a homogenized model of the plate, made of bi-dimensional shell elements (*elements S4R* [23]). Such elements were directly characterized with the stiffness parameters of the homogenized plate, according to the constitutive law expressed in (1). Stiffness parameters in morphing directions were evaluated by performing tensile and bending analyses on the complete detailed model that has been previously described. The homogenized shell model was analyzed by applying the same stretching and the same pressure loads considered for the detailed model, including the effects of geometrical non-linearity. The vertical deflection measured at the nodes of the homogenized model represents the overall bending response, which was subtracted to the vertical displacements of the external elastomeric cover obtained in the FEM analysis of the detailed model, to quantify the waviness effect.

A typical deformed shape obtained in a tensile analysis on the detailed model is shown in figure 11-(a), which presents the contour of maximum principal strains in all the elements of the systems. The profile shown in figure 11-(b) is referred to tensile stretching, whereas the one in figure 11-(c) is referred to the compressive case. The critical condition for waviness is tension, because the lower horizontal arms deflect upwards and push the honeycomb, which induces the local deflection of the elastomeric skin in the supported region, whereas the part bonded to the upper horizontal arm experiences a smaller vertical displacement. Such phenomenon originates the bands observed in figure 9-(c). The numerical vertical displacements of the external surface in the detailed model (DM) and the overall bending obtained in the analysis of the homogenized shell model (HM) under the same load conditions are presented in figure 12 for the 12% tensile stretch case, at increasing values of applied pressure.

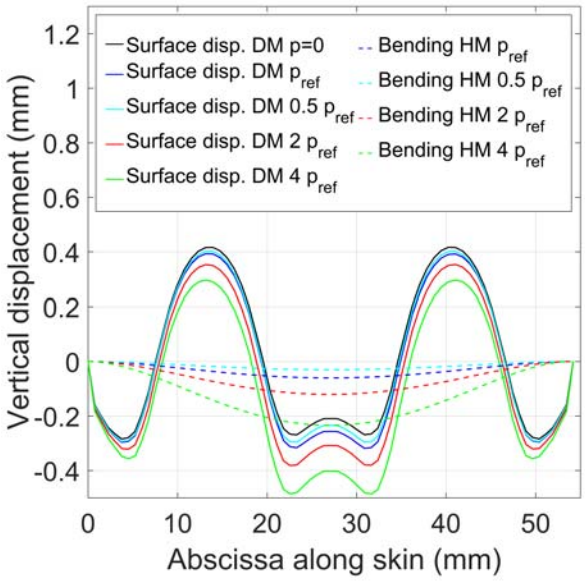

Figure 12. Profiles of vertical surface displacements in analyses of the model stretched at 12% at different pressure levels

The absolute value of displacements is below 0.5 mm. It can be observed that the maximum differences between surface displacements in the detailed model and overall bending behavior are due to aforementioned interaction between the honeycomb insert and the lower horizontal arm of the corrugated laminate. The major effect of increasing pressure is related to overall bending, whereas the surface profile remains qualitatively unchanged.

A series of analyses was also performed by removing the honeycomb inserts in the detailed model. In the plot reported in figure 13, waviness is quantified as the absolute value of the difference Δ_z between the maximum surface displacement in the detailed model and the displacement of the homogenized model taken at the same point. The trend of Δ_z is reported for increasing pressures and different types of analyses. If honeycomb is removed, waviness increases with pressure up to values higher than 1.5 mm for $p = 4p_{ref}$. Tensile stretching modifies the waviness and the slope of the waviness-pressure curve. However, stretching has no dominant effects. When honeycomb is applied, the effect of pressure on the waviness is significantly reduced. Without stretching, Δ_z is lower than 0.1 mm for any pressure value, but a tensile stretching of 12% leads to a waviness of about 0.4 mm. However, it can be observed that, in the stretched solution with honeycomb, waviness is actually reduced if pressure is increased.

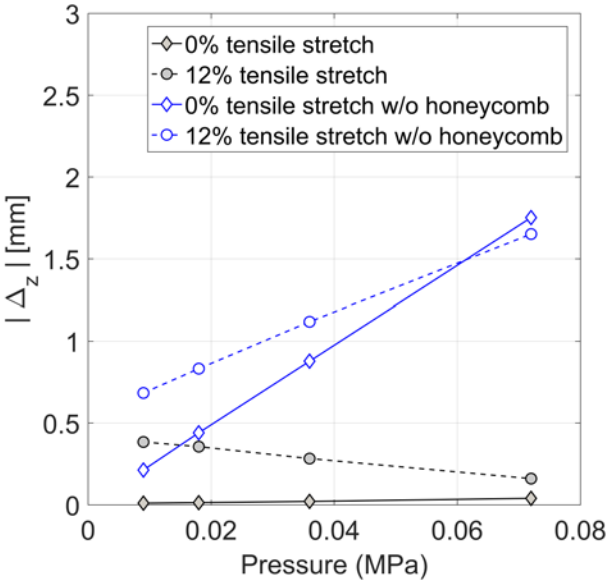

Figure13. Waviness of different skin systems at increasing pressures

Assuming that surface irregularities have to be kept below 1% of the chord to avoid excessive detrimental aerodynamic effects, as proposed in [10], a chord of 1200 mm would be required if the 12 mm deep valleys of the corrugated laminate were not covered by any additional layer. The proposed system drastically reduces the required chord length to fulfill such requirement, since a chord of 50 mm is adequate for the worst considered case, which occurs for a skin stretching of 12%. It should be remarked such stretching is indeed a very high value for most of the morphing applications considered in literature. Moreover, such reduction of waviness is obtained without completely filling the corrugated laminates with elastomeric material, which would lead to a very high weight penalty. Accordingly, the proposed technological solutions can be considered adequate to obtain an aerodynamically efficient skin, still maintaining all the advantages of corrugated laminates.

4. Numerical performances indices of skins based on square-shaped corrugated laminates

4.1. Configurations based on square-shaped cells and performance indices

In the previous sections, a technological process has been presented to produce square-shaped corrugated laminates and to integrate an external aerodynamically efficient elastomeric skin. As it was shown in section 2.3, two square-shaped corrugated profiles can be bonded along the horizontal straight arms

to obtain a more complex shape, a twin corrugated laminate. Indeed, another possible configuration, which will be referred to as doubled corrugated laminate, can be obtained by bonding two corrugated laminates with different periods. Such types of geometry was also proposed in [19, 20]. These three possible configurations are shown in figure 14. It should be remarked that all of them are suited to be endowed with the elastomeric skin supported by honeycomb stripes. The twin and doubled corrugated laminates are characterized by the presence of closed cells, which can provide several advantages, since they make available a well-protected environment to host sensors, diffused actuation systems and damping media. Generally, it is expected that the three configurations proposed in figure 14 achieve different mix of properties, such as a different ratio between axial and bending stiffness, and that each geometry could presents specific advantages and drawbacks with respect to the others.

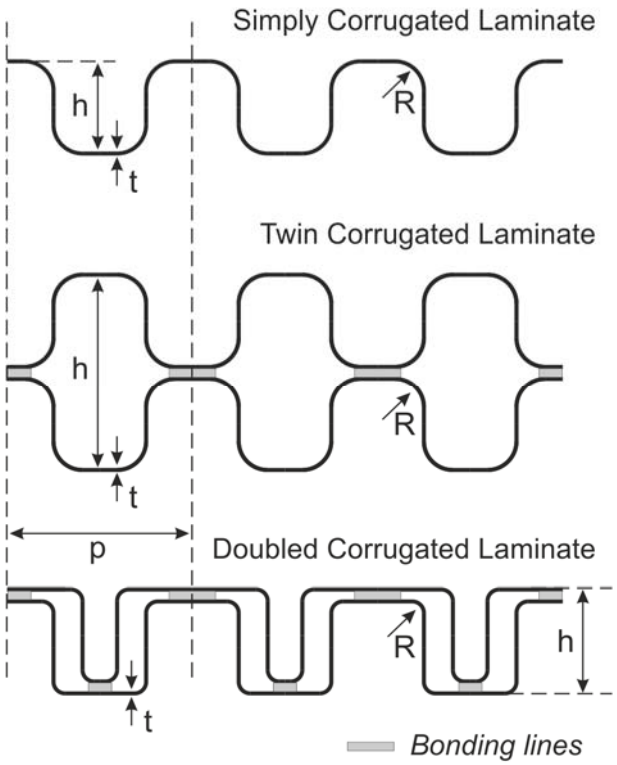

Figure 14. *Configuration based on square-shaped corrugated laminates*

Therefore, the properties in morphing and non-morphing directions of the proposed configurations were numerically analyzed by developing parameterized finite element models of the unit cell for each configuration. All meshes were obtained by using a typical element length of 0.5 mm and were generated by using 8-noded continuum shell elements. Hence, the modelling approach is the one applied to simple

and twin corrugated profiles in figure 5-(b,c), which was correlated with experimental results in figure 6. Since this numerical study is mainly aimed at comparing the performances of the different configurations, an homogeneous lay-up of fabric plies, $[0]_n$, was considered. The property of the plies are the ones reported in table 2.

The first index that was evaluated is the axial stiffness in the morphing direction, $\bar{A}_{11}$. A one-element wide strip of the unit cell was generated, as the one presented figure 15-(a), referred to the simple corrugated laminate. Rotation was constrained at the ends of the unit cell and two horizontal forces were applied to stretch the unit cell. A second performance index is referred to the bending stiffness in the morphing direction. The same type of model adopted for axial stiffness was used, but two bending moments were applied at the ends, as it shown in figure15-(b), which is referred to doubled corrugated laminate. The relative rotation at the free end, ϑ_y, was acquired and bending stiffness $\bar{D}_{11}$ was calculated. The ratio between the bending stiffness in the morphing direction and the axial stiffness $\bar{D}_{11}/\bar{A}_{11}$ was considered an important functional performance index for the morphing skin, since many applications require adequate bending stiffness to sustain aerodynamic loads but low axial stiffness to allow large shape variations with low actuation force levels.

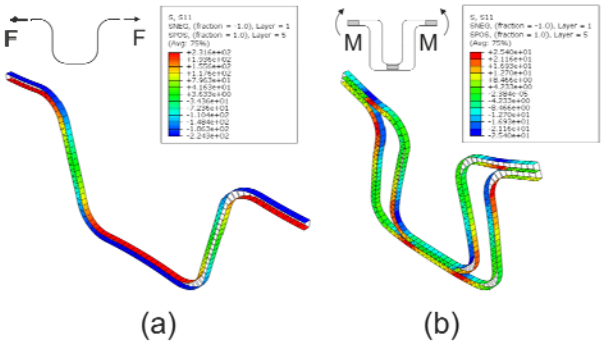

Figure 15. Examples of tensile (a) and bending (b) analyses for properties in morphing direction

Among the properties in non-morphing directions, bending stiffness $\bar{D}_{22}$ and the in-plane shear stiffness $\bar{A}_{66}$ were evaluated by developing parameterized three dimensional models of the representative unit cell, with a length, *L*, and a width, *w*, such that $L = w = p$, where *p* is the period of the corrugation.

An example of bending analysis in non-morphing direction is presented in in figure 16-(a), for a doubled corrugated laminate. Two reference nodes were created at the two opposite faces and were connected by a kinematic link to the nodes of the corresponding face. This link imposed that the end sections of the model, initially plane, remain plane. A bending moment was applied to the reference nodes at both ends of the model and the stiffness $\overline{D}_{22}$ was computed by evaluating the relative rotation between the two faces.

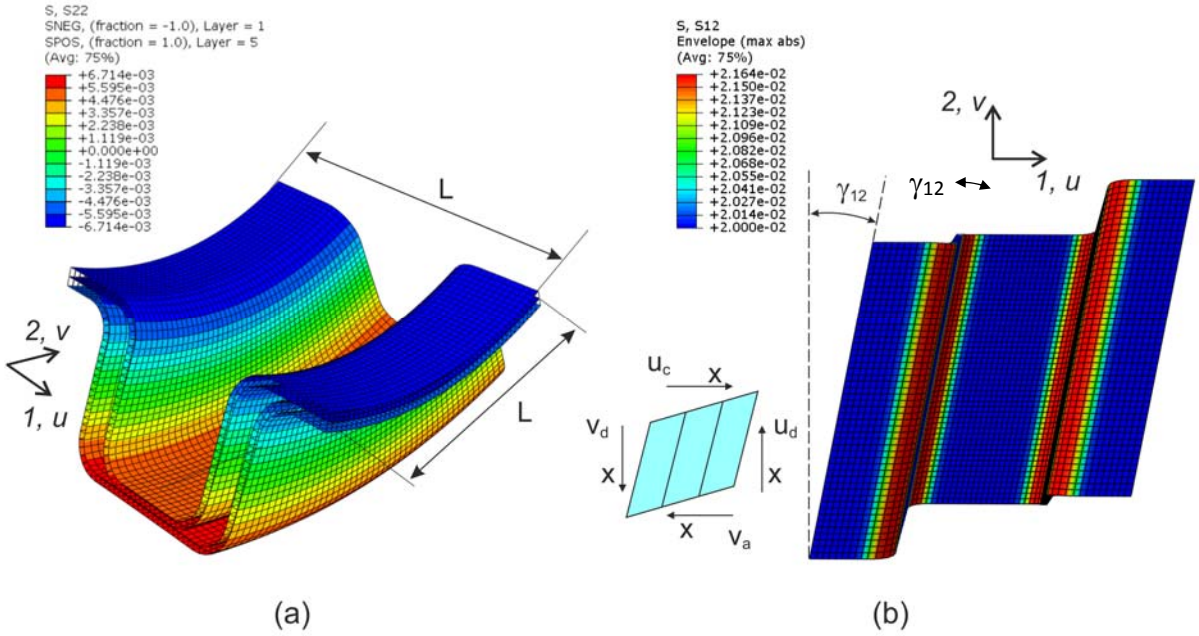

Figure 16. Analyses for bending in non-morphing direction (a) and shear response (b)

A normalized structural index was then defined, by calculating the ratio between $\overline{D}_{22}$ and the bending stiffness of a flat laminate made of the same material and having the same areal density of the corrugated profile. The weight of the support was calculated from the finite element model generated by the automatic procedure and the thickness of the equivalent flat laminate, t_{eq}, was determined by simple geometrical considerations. Then, the normalized bending structural index reads:

$$K_b = \overline{D}_{22} \Big/ \left(\frac{t_{eq}^3}{12} \frac{E_b}{1-\nu_{12}^2} \right) \tag{5}$$

where E_b is the equivalent bending Yonug modulus of the flat laminate. Since it is assumed that the flat laminate has the same ply properties, that the lamination sequence is an homogeneous lay-up $[0]_n$ and that both corrugated and flat plate undergoes cylindrical bending, modulus E_b is the Young modulus of the ply, reported in table 2, in the morphing direction.

The second index referred to properties in non-morphing direction is related to the in-plane shear stiffness, which was evaluated by applying a displacement-controlled analysis to the three dimensional models. In such analyses, the nodes belonging to each side of the representative cells were linked to four reference nodes, shown in figure 16-(b). Equations were used to link the horizontal displacements u of the horizontal boundaries and the vertical displacement v of the vertical boundaries to the corresponding ones of the reference nodes, $u_{a,c}$ and $v_{b,d}$, respectively. Then, a displacement boundary condition was applied, such that $u_a = v_b = u_c = v_d$. In such conditions, the system of reaction forces acting on the reference nodes corresponds to a shear load with a magnitude F. By evaluating the angle γ_{12}, the in-plane shear stiffness $\overline{A}_{66}$ of the support can be determined. A normalized shear structural index was defined by considering a flat laminate with homogeneous $[0]_n$ lay-up and thickness t_{eq}, which was evaluated considering a flat panel with the same weight of the corrugated laminate:

$$K_s = \overline{A}_{66} \Big/ \left(G_{12} t_{eq} \right) \tag{6}$$

4.2. Set up and results of numerical sensitivity study

Parameterized models of the configurations based on square-shaped corrugated laminates were generated by varying geometrical parameters including height, h, period, p, fillet radius, r, and thickness, t. The main objectives of such study were the evaluation of the performances indices $\overline{A}_{11}$, $\overline{D}_{11} \big/ \overline{A}_{11}$, K_b and K_s for different geometries and the comparison between the performances of the three configurations. The index $\overline{D}_{11} \big/ \overline{A}_{11}$ is negligibly affected if lay-up is changed, since both stiffness parameters mainly depend on bending stiffness of the composite laminate. Moreover, also the indices K_b and K_s are actually not affected by the lay-up, assuming a homogeneous orientation of the fibers and identical ply properties

both in the corrugated laminate and in the flat laminate used to normalize the stiffness. Therefore, the homogeneous lay-up $[0]_n$ was maintained for all the models.

It is worth noting that in the twin and doubled corrugated configurations presented in figure 14, the length of the bonding line represents an additional design variable that requires some additional considerations. Indeed, in the twin corrugated configuration, the zones where the simply corrugated laminates are bonded together at the neutral plane of the twin laminate and do not provide a significant contribution neither to axial compliance, neither to the bending stiffness in morphing and non-morphing direction. It should also be noted that a limited bonded length for the twin and doubled configuration also reduces the unsupported lengths of the external elastomeric cover in the 'valleys' of the corrugated shape, thus reducing the need of large honeycomb supports. Accordingly, the lengths of the bonded zones were set to a relatively small fixed length of 5 mm in all the performed parametric studies that were performed.

The availability of parameterized finite element models allowed building the response surfaces for all the properties in morphing and non-morphing directions, considering the variability ranges reported in table 5. A full factorial grid in the four-dimensional space (*h*,*p*,*r*,*t*) was used, with 6 points along each dimension.

Table 5. Variability range of design parameters and points for section visualization

	Min Value	Max Value	P1	P2	P3	P4	P5
t (mm)	0.50	1.50	0.50	0.75	1.00	1.25	1.50
r (mm)	2.00	3.00	2.00	2.25	2.50	2.75	3.00
p (mm)	20	32	20	23	26	29	32
h (mm)	12	20	12	14	16	18	20

Examples of response surface sections, in the plane *h*-*p* are reported in figure 17 for t =1 mm and r = 3 mm. Indeed, axial and bending stiffness in morphing direction mainly depend on the bending behavior of corrugated walls, so that they typically depend on t^3 for all the considered geometries. The analyses

of figure 17, indicate that, for the axial stiffness, $\overline{A}_{11}$, a dominant parameter is the height, *h*, whereas the period, *p*, has small or negligible influence, as it is exemplified in figure 17-(a), referred to a simply corrugated shape. Both period and height affect the bending stiffness $\overline{D}_{11}$ for all the geometries, though the effect of *h* is typically higher. The ratio of bending stiffness to axial stiffness, $\overline{D}_{11}/\overline{A}_{11}$ is presented in figure 17-(b) for the Doubled Corrugated Laminate, which presents the highest values for such parameter. The influence of both height and period can be appreciated.

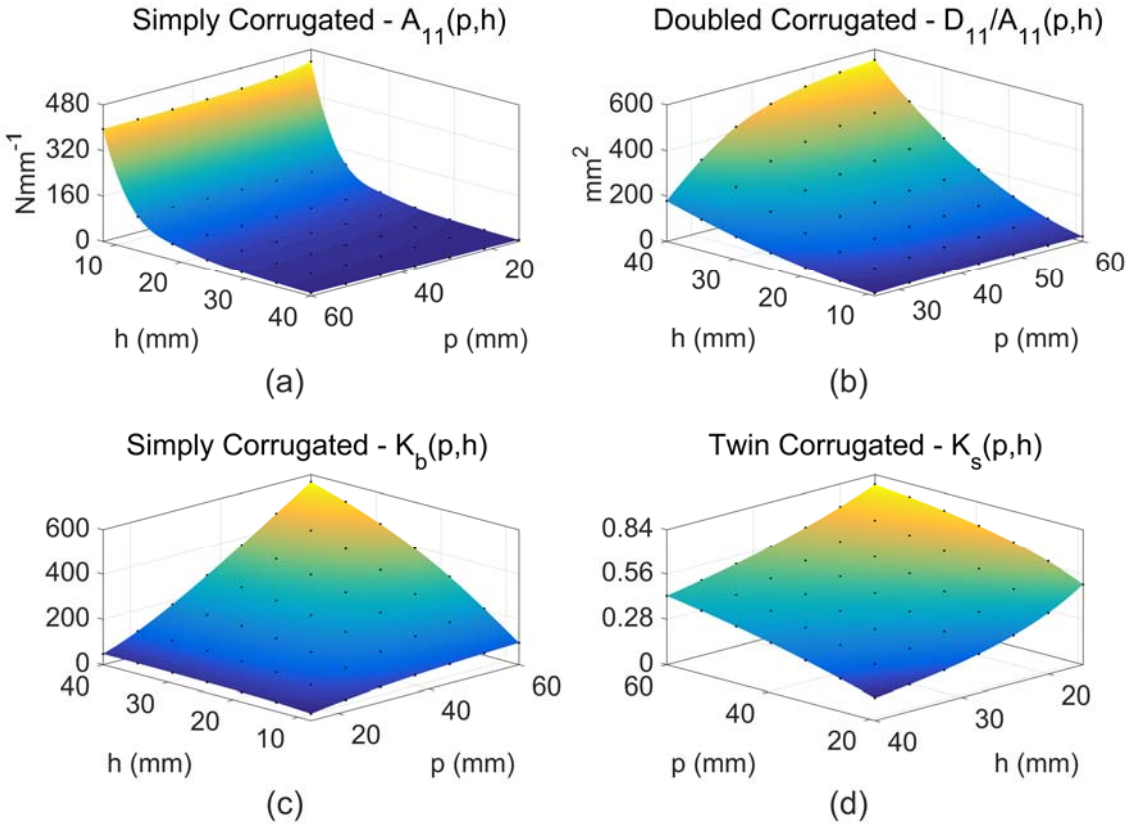

Figure 17. Example of response surface of axial stiffness (a), bending to axial stiffness ratio (b), bending in non-morphing direction index (c), and in-plane shear stiffness index (d) for different corrugated configurations

The bending structural index, K_b, is typically very high, because corrugations increase the moment of inertia of the sections with respect to the flat panel having identical weight. Actually, the thickness of the sides is the most important parameter affecting such index, but the effect of both period and height is not negligible, as it can be observed in figure 17-(c), referred to a simply corrugated laminate. The qualitative trend for the other geometries is very similar. The normalized shear stiffness index, K_s, is

typically lower than unit, as it is exemplified in figure 17-(d), referred to a twin corrugated laminate. This can be explained by observing the mechanism of shear deformation represented in figure 16-(b). Shear stress acts in the vertical sides of the corrugated laminate and gives a contribution to the shear angle γ_{12}, without providing a contribution to the resultant in-plane shear force F. For such a reason, the index increases as h is reduced for all the considered geometries, whereas both bending stiffness in morphing and non-morphing directions exhibit the opposite trend.

In table 5, the location of five points P1, P2, P3, P4 and P5 in the space of design variables is also provided. The plots in figure 18 represent the sections passing through the central point P3 of the $\overline{D}_{11}/\overline{A}_{11}$ response surface, taken along the axes t, p, h, r and sampled at points P1,P2, P3, P4, P5. Such representation allows appreciating the influence of the different design variables and provides a quantitative indication of the values that the different performance indices can obtain for the different corrugation configurations. It can be observed that height h has the most significant influence on the functional index $\overline{D}_{11}/\overline{A}_{11}$, which represents the possibility to maintain an adequate bending stiffness with an high axial compliance. The doubled corrugated laminate presents the highest values for such index. Actually, the analysis of the whole response surface indicates that the differences in $\overline{D}_{11}/\overline{A}_{11}$ values between the doubled corrugated geometry and the other two configurations can be even greater than the ones referred to the sections presented in figure 18. Moreover, such configuration exhibits a significant variation of the $\overline{D}_{11}/\overline{A}_{11}$ index with other parameters, namely t, r and p, thus indicating a significant design flexibility.

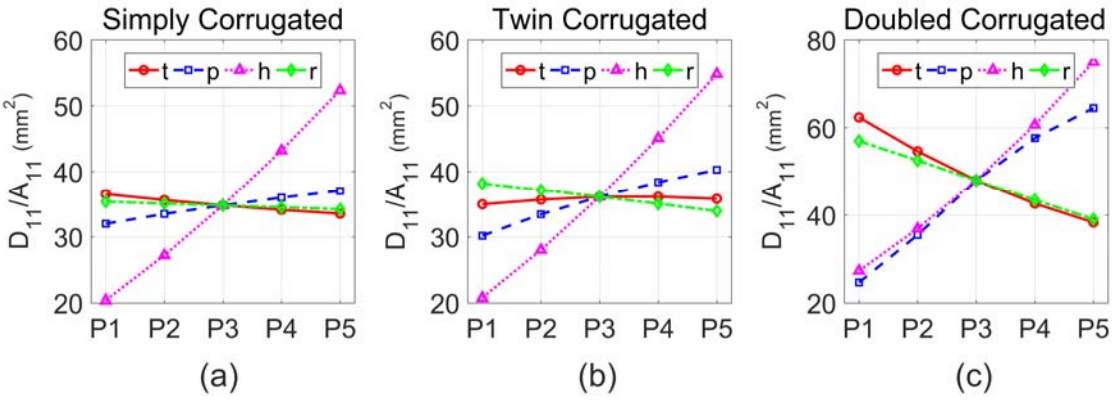

Figure 18. Sections along the axes of design variable space for the D_{11}/A_{11} response surface of simply corrugated (a), twin corrugated (b), and doubled corrugated (c) configurations

Although the doubled corrugated laminates offer the highest $\overline{D}_{11}/\overline{A}_{11}$, the minimum axial stiffness is obtained by using simply corrugated shapes, as it is shown in figure 19. It can be seen that, for the same values of parameters, the axial stiffness exhibited by the simple corrugated laminate is about one order of magnitude lower than the one of twin corrugated configurations and three times lower than the one obtained by the doubled corrugated laminates. However, the absolute value of axial stiffness can be modified by changing thickness or ply orientations.

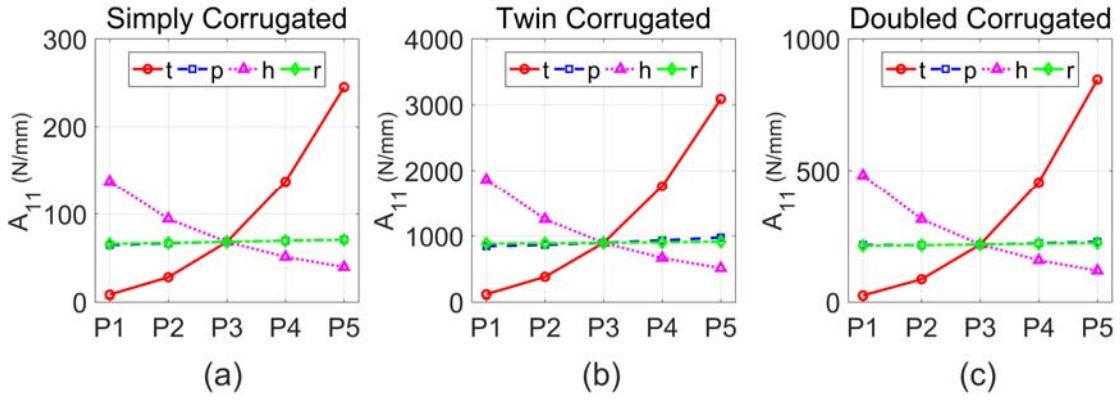

Figure 19. Sections along the axes of design variable space for the A_{11} response surface of simply corrugated (a), twin corrugated (b), and doubled corrugated (c) configurations

Sections sampled at the points indicated in table 5 also make possible a comparison between the different geometries for the structural indices in non-morphing direction, K_b and K_s, which represent bending and shear stiffness normalized with respect to the ones of a panel having the same weight of the corrugated laminates. Considering the structural index K_b, the sections reported in figure 20 confirm that thickness is the most significant variable affecting the index. The influence of the other parameters, is actually much less important, from a quantitative standpoint. The simply corrugated laminates achieve the highest values for such index, which, in the considered sections, are about two times the ones of the twin corrugated laminates and three times the ones of the doubled corrugated configurations.

The structural index K_s is particularly important for morphing skins, since skin contribution to shear stiffness is one of the most important features of stressed skin constructions used in aerospace applications. In the plots presented in figure 21, it can be seen that all design variables have a significant influence on this index. However, the effect of height variable, which was previously commented, is dominant. It can be observed, for the considered sections, that twin corrugated laminates present the highest value of such index. Overall, data analysis indicate that shear structural index and axial compliance are conflicting performance indices, so that the configurations presenting the lowest compliance are also the ones that obtain the lowest shear stiffness contributions. However, sections show that it is possible to manufacture a morphing skin that can exhibit a shear stiffness from 20% to 70% of the ones of a flat panel made of identical material and with identical weight.

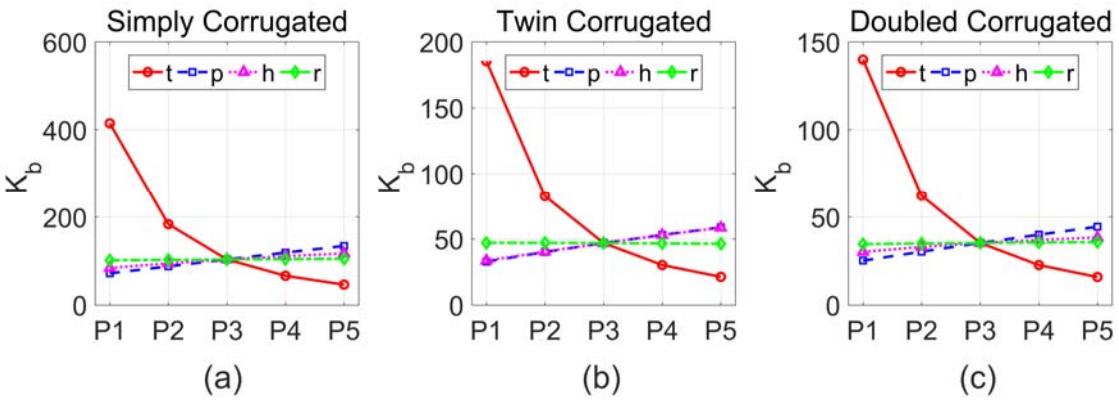

Figure 20. Sections along the axes of design variable space for the K_b response surface of simply corrugated (a), twin corrugated (b), and doubled corrugated (c) configurations

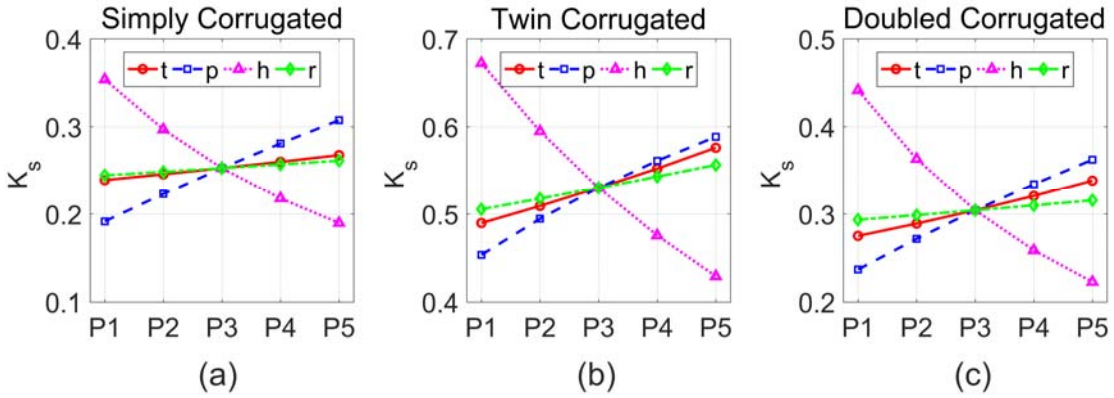

Figure 21. Sections along the axes of design variable space for the K_s response surface of simply corrugated (a), twin corrugated (b), and doubled corrugated (c) configurations

5. Conclusions

This work proposes design and technological solutions for the development of a morphing skin that can fulfill several critical requirements related to its aerodynamic and structural functions. The activity carried out to set up the manufacturing process for the production of square-shaped corrugated laminates, with rounded fillets, provided the guidelines for the achievement of good quality laminates and assessed different types of analytical and numerical approaches for stiffness prediction. The square shaped corrugated configuration proposed in this work presents straight horizontal arms that are well suited for integration of additional elements in the skin system and for the combination of different laminates to obtain new geometries. In particular, a technological solution to integrate an elastomeric cover in the corrugated laminate at a moderate weight cost was presented, with the objective of producing a smooth and aerodynamically efficient surfaces. Experiments and numerical results show that such integration can be accomplished without altering the mechanical properties of the corrugated laminate and that surface waviness can be drastically reduced with respect to the original corrugated profile. It is important remarking that, in the solution proposed, the tearing or the failure of the external aerodynamic cover will not lead to the loss of the load carrying capabilities of underlying corrugated laminate, whereas the external elastomeric layer represents a protection against foreign object impacts for the corrugated structural support. Combinations of square-shaped corrugated laminates were also proposed, which can also be endowed with the elastomeric cover to obtain aerodynamically efficient skins. Performances indices based on the bending to axial stiffness ratio in morphing direction and on structural contributions in non-morphing directions were introduced, taking in consideration the weight cost involved in the adoption of the morphing corrugated skin. The development of parameterized models, adopting a numerical approach validated with experimental tests, made possible the investigation of performance indices considering wide range of variations of the main geometrical parameters. Results identify that the simply corrugated shape exhibits the lowest axial stiffness and maximize, for a given areal weight, the bending

stiffness in non-morphing direction. However, combined corrugated laminates achieve maximum bending to axial stiffness ratio and maximum structural efficiency for shear stiffness. Such configurations are also characterized by closed cells that are well-suited to host sensors, actuation systems, de-icing devices and other type of systems to develop a multi-functional stressed skin. Overall, the work confirm the potential of square-shaped corrugated composite laminates to design morphing skin and proposes innovative and promising solutions to develop aerodynamically efficient skins and new corrugated configurations that can be exploited to enhance the structural and multi-functional performances of the skin in new architectures, specifically designed for morphing.

Acknowledgements

The authors wants to thanks the inter-departmental laboratory AMALA of Politecnico di Milano for the co-operation.

Appendix A: Application of Timoshenko beam theory to square-shaped corrugated laminates

The evaluation of the axial and bending stiffness reported in Eq. 2 was obtained by applying Timoshenko beam theory to the corrugation profile. Assuming that the laminate undergoes cylindrical bending, the corrugated profile can be considered like a beam of unit width with a rectangular section of height *t*, so that section area is A=1 x t. The kinematic hypothesis of the theory involves plane sections that remain planes in the deformation process and rotates of an angle ψ due to bending and of an angle γ due to transverse shear. Deformation mechanism is sketched in figure A1. Thanks to symmetry considerations, the analysis can be limited to the analytical area that has been evidenced in figure 1-(b). Figure A1 is referred to the calculation of the axial stiffness, which requires the evaluation of the displacement δ_x under the action of the force F_x. The profile is divided into three parts and the problem is set up by introducing the axial, vertical and rotational displacements along the axis of the beam, which are shown in figure A1 for the three domains.

The differential equations governing the structural problem and the relevant boundary conditions for the application of force F_x are reported in (A1), (A2), and (A3) for each domain, including the essential and

the natural boundary conditions. In the equations, a shear correction factor, k = 5/6, was introduced to more accurately represent the transverse shear stiffness of the beam chunks. The formulation for the curved Timoshenko beam in the second domain, reported in (A2), was derived following [25]. Eventually, equation solution makes possible the evaluation of $v_3(l) = \delta_x$, so that the axial stiffness can be determined, thus leading to the analytical result reported in the first of equations (2). Application of a bending moment to the free end of the analytical area leads to a second set of equations that allows the evaluation of the rotation at the free end and of the bending stiffness reported in the second line of equation (2). In this second case, all beams are in pure bending conditions and no effect of transverse shear stiffness is observed.

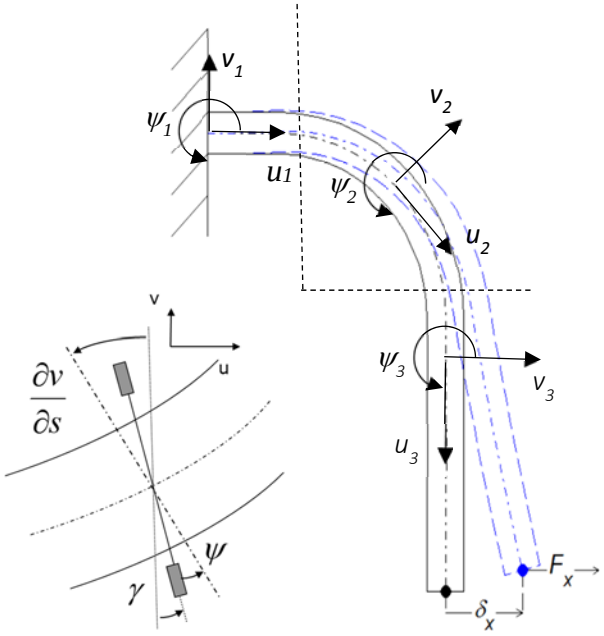

Figure A1. Sections along the axes of design variable space for the K_s response surface of simply corrugated (a), twin corrugated (b), and doubled corrugated (c) configurations

$$\begin{cases} EAu_1''(s) = 0 \\ kGA\left[v_1''(s) - \psi_1'(s)\right] = 0 \\ kGA\left[v'_1(s) - \psi_1(s)\right] + EI\psi_1''(s) = 0 \end{cases} \quad \begin{cases} u_1(0) = 0 \\ v_1(0) = 0 \\ \psi_1(0) = 0 \end{cases} \quad \begin{cases} EI\psi_1'(b) = F_x(l+r) \\ EAu'(b) = F_x \\ kGA\left[v_1(b) - \psi_1(b)\right] = 0 \end{cases} \tag{A1}$$

$$\begin{cases} EA\left[u_2''(s)-\dfrac{v'_2(s)}{r}\right]-\dfrac{kGA}{r}\left[v'_2(s)-\psi_2(s)+\dfrac{u_2(s)}{r}\right]=0 \\ kGA\left[v''_2(s)-\psi'_2(s)+\dfrac{u'_2(s)}{r}\right]+\dfrac{EA}{r}\left[u'_2(s)-\dfrac{v_2(s)}{r}\right]=0 \\ kGA\left[v'_2(s)-\psi_2(s)+\dfrac{u_2(s)}{r}\right]+EI\psi''_2(s)=0 \end{cases} \tag{A2}$$

$$\begin{cases} u_2(0)=u_1(b) \\ v_2(0)=v_1(b) \\ \psi_2(0)=\psi_2(b) \end{cases} \quad \begin{cases} EI\psi_2(\pi r/2)=F_x l \\ u'_2(\pi r/2)-\dfrac{v_2(\pi r/2)}{r}=0 \\ kGA\left[v'_2(\pi r/2)-\psi_2(\pi r/2)+\dfrac{u_2(\pi r/2)}{r}\right]=F_x \end{cases}$$

$$\begin{cases} EAu_3''(s)=0 \\ kGA\left[v_3''(s)-\psi_3'(s)\right]=0 \\ kGA\left[v'_3(s)-\psi_3(s)\right]+EI\psi_3''(s)=0 \end{cases} \quad \begin{cases} u_3(0)=0 \\ v_3(0)=0 \\ \psi_3(0)=0 \end{cases} \quad \begin{cases} EI\psi_1'(l)=0 \\ EAu'(l)=0 \\ kGA\left[v'_3(l)-\psi_3(l)\right]=F_x \end{cases} \tag{A3}$$

Appendix B: Characterization of the hyperelastic material model for the elastomeric cover

The characterisation of the hyperelastic constitutive law used in the detailed model of the skin, required two different tests for the definition of the coefficient of strain energy potential reported in (4). In a first test (uniaxial test) material was let free to laterally contract during tension, whereas, in the second test, the lateral contraction was opposed by stretching a relatively short and large specimen, fully clamped at the upper and lower end (planar test).

The uniaxial tensile test was carried out according to regulation ASTM D638 (specimen type IV) [26]. Three dog-bone shaped specimens with a gauge length of 25 mm and a width of the narrow section of 6 mm and a thickness of 4 mm were cut and tested under displacement control at three different velocities: 5 mm/min, 50 mm/min and 500 mm/min. A phase of the test is shown in figure B1-(a). For the planar tensile test, no specific regulations are available. The objective of the test is obtaining a state of pure shear at 45° with respect to tension direction. This is achieved by using a specimen with a very high width to height ratio, so to avoid the lateral contraction of the nearly incompressible elastomeric material. The adoption of a 0.25 width to height ratio is known to be optimal to accomplish such objective [27]. Accordingly, specimens with a thickness of 2 mm, a width of 140 mm, and a gauge length of

35 mm were adopted to perform tests at 5 mm/min, 50 mm/min and 500 mm/min. A phase of the test is shown in figure B1-(b). Differences exist between the responses at different loading rates, although they are relatively limited.

The responses at 5 mm/min reported in figure B1-(c) were used to calibrate different forms of the hyperelastic potentials, available in the Simulia/Abaqus code [23]. The second order form of the Odgen strain energy potential, given in (4) obtained the best fitting for the two tests and was therefore selected. The best fitting procedures included in the solver code provided the material parameters reported in table 4.

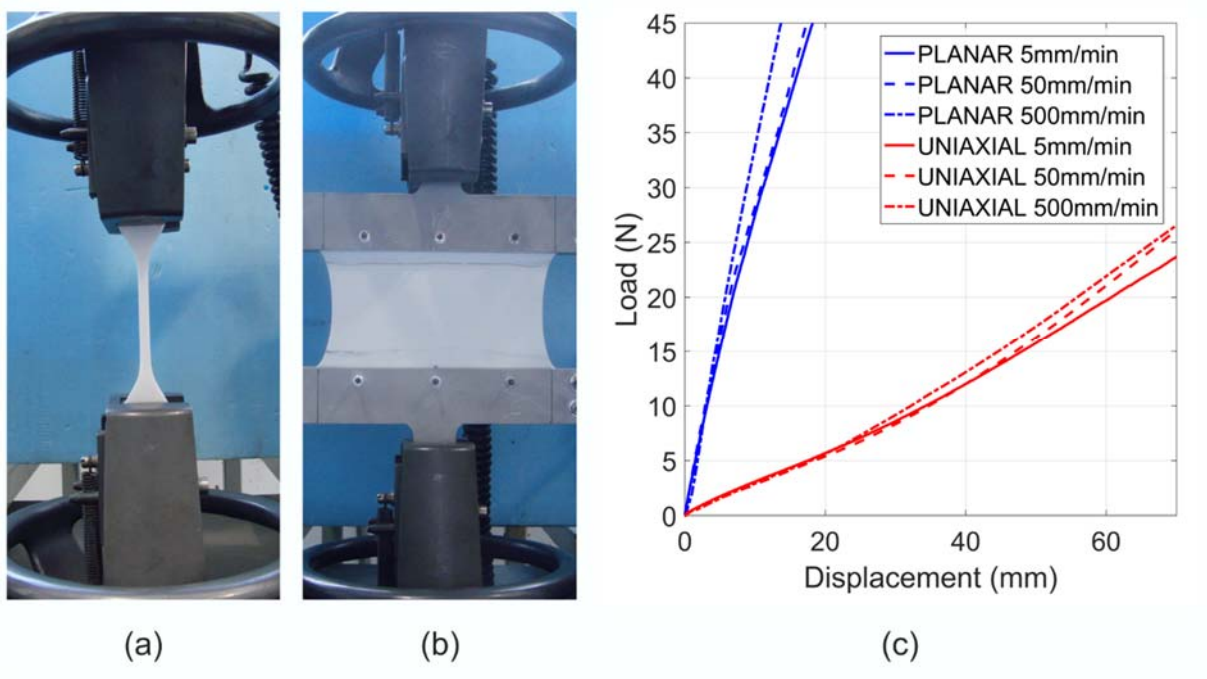

Fig. B1. Uniaxial (a) and planar (b) tensile tests performed on the silicon elastomer and force vs. displacement responses (c)

References

[1] Barbarino S, Bilgen O, Ajaj RM, Friswell MI and Inman DJ 2011 A review of morphing aircraft *Journal of Intelligent Material Systems and Structures* **22** 823-827

[2] Sofla AYN, Meguid MA, Tan MA, Yeo WK 2010 Shape morphing of aircraft wing: Status and challenges *Materials and Design* **3**, 1284-1292

[3] Gandhi F and Anusonti-Inthra P 2008 Skin design studies for variable camber morphing airfoils *Smart Materials and Structures* **17** 1-8

[4] Heintze O, Steeger S, Falken A and Heckmann J 2016 Enhanced adaptive droop nose: from computer model to multli-functional integrated part, in: *Smart Intelligent Aircraft Structure (SARISTU): Proceedings of the Final Project Conference*, Woelchen PC and Papadopoulos M editor, Springer International Publishing 97-111

[5] Kintscher M, Kirn J, Storm S, Peter F 2016 Assessment of the SARISTU enhanced adaptive droop nose, in: *Smart Intelligent Aircraft Structure (SARISTU): Proceedings of the Final Project Conference*, Woelchen PC and Papadopoulos M editor, Springer International Publishing 113-140

[6] Yokozeki T, Takeda S, Ogasawara T. and Ishikawa T 2006 Mechanical properties of corrugated composites for candidate materials of flexible wing structures Composites: Part A **37**, 1578-1586

[7] Thill C, Etches J, Bond IP, Potter K and Weaver P 2007 Corrugated composite structures for aircraft morphing skin applications *Proceedings of the 18th international conference of adaptive structures and technologies. Ottawa, Ont., Canada, October 3rd-5th 2007*

[8] Thill C, Etches J, Bond IP, Potter K and Weaver P, 2008 Morphing Skins *The Aeronautical Journal* **112** 117-139

[9] Thill C, Etches J, Bond IP, Potter K and Weaver P 2010 Composite corrugated structures for morphing wing skin applications *Smart Material and Structures* **19** 1-10

[10] Thill C, Downsborough JD, Lai SJ, Bond IP and Jones DP 2010 Aerodynamic study of corrugated skins for morphing wing applications The Aeronautical Journal **114** 237-44

[11] Xia, Y, Bilgren O, Friswell MI 2014 The effects of corrugated skins on aerodynamic performances *Journal of Intelligent Material Systems and Structures* **25(7)** 786-794

[12] Kress G and Winkler M 2010 Corrugated laminate homogenization model *Composite Structures* **92(3)** 795-810

[13] Ghabezi P and Golzar M 2013 Mechanical analysis of trapezoidal corrugated composite skins *Applied Composite Materials* **20** 341-353

[14] Winkler M and Kress G 2012 Influence of corrugation geometry on the substitute stiffness matrix of corrugated laminates *Composite Structure* **94** 2827-2833

[15] Airoldi A, Crespi M, Quaranta G and Sala G 2012 Design of a morphing airfoil with composite chiral structure. *Journal of Aircraft,* **49(4)** 1008-1019

[16] Airoldi A, Bettini P, Panichelli P, Oktem MF and Sala G 2015 Chiral topolgies for composite morphing structures – Part I: Development of a chiral rib for deformable airfoil *Physica Status Solidi b* **252(7)** 1435-1445

[17] Xia Y, Friswell, MI and Saavedra Flores EI 2012 Equivalent models of corrugated panels, International Journal of Solids and Structures **49** 1453-1462

[18] Kress G and Winkler M 2011 Corrugated laminate analysis: a generalized plane strain problem *Composite Structures* **93** 1493-1504

[19] Fournier S, Airoldi A, Borlandelli E and Sala G. 2013 Flexible Composite Supports for Morphing Skins *Proceedings of XXII Conference of Italian Association of Aeronautics and Astronautics* , Naples, Italy, 9-12 Sept. 2013

[20] Previtali F, Molinari G, Arrieta AF, Guillaume M and Ermanni P 2016 Design and experimental characterisation of a morphing wing with enhanced corrugated skin *Journal of Intelligent Materials and Structures* **27** 278-292

[21] Xia Y, Bilgren O, and Friswell MI 2014 The effects of corrugated skins on aerodynamic performances *Journal of Intelligent Material Systems and Structures* **25(7)** 786-794

[22] Schmitz A, Horst P 2014 Bending deformation limits of corrugated unidirectionally reinforced composites Composite Structures **107** 103-111

[23] Abaqus, 2012 Analysis User Maual Version 6.12 *Dassault System*

[24] Odgen RW, 1972 Large deformation isotropic elasticity – on the correlation of theort and experiments for incompressible rubberlike solids *Proceedings of the Royal Society of London, Series A, Mathematical and Physical Sciences* **326(1567)** 565-584

[25] Lee SY, Yan QZ, 2015 Exact Static Analysis of In-Plane Curved Timoshenko Beams with Strong Nonlinear Boundary Conditions *Mathematical Problems in Engineering* **2015** doi:10.1155/2015/646391

[26] ASTM Standard D638, 2014, Standard Test Method for Tensile Properties of Plastics, ASTM International, West Conshohocken, PA, 2003, DOI: 10.1520/C0033-03, www.astm.org.

[27] Palmieri G, Sasso M, Chiappini G and Amodio D 2011 Virtual fields method on planar tension tests for hyperelastic materials characterisation *Strain* **47(2)** 196-209